Electronic Supporting Information

Heteroleptic Cu(II) saccharin complexes: intriguing coordination modes and properties

Gloria Mazzone, Emilia Sicilia, Elisabeta I. Szerb, Massimo La Deda, Loredana Ricciardi, Emilia Furia, Barbara Sanz Mendiguchia, Francesca Scarpelli, Alessandra Crispini and Iolinda Aiello

Table of Contents

- Experimental Section **p. 2**
- **Fig. S1** Apparatus for preparation of saturated complex solutions **p. 3**
- **Fig. S2** Absorption spectrum for the **1a**, **1** and **2** **p. 4**
- **Table S1** Details of data collection and structure refinements for **1a-1** and **2a-2b** **p. 6**
- **Fig. S3** ^{1}H-NMR spectrum of **1a** **p. 8**
- **Fig. S4** ^{1}H-NMR spectrum of **1** **p. 8**
- **Fig. S5** ^{1}H-NMR of **2** **p. 9**
- **Fig. S6** Absorption spectra of tropolone and bipyridine in water solution at room temperature **p. 9**
- **Fig. S7** Comparison between the X-ray powder pattern (black) measured on the pale-blue powder of **1a**, (blue) calculated from the single crystal data and (red) measured on the needle-shaped microcrystals **p. 10**
- **Table S2** Selected bond distances (Å) and angles (°) of **1** and [(bipy-OH)Zn(Trop)(Cl)] **p. 10**
- **Fig. S8** Comparison between the X-ray powder pattern (black) calculated from the single crystal data of **1** and (red) measured on blue powder **p. 11**
- **Table S3** Selected bond distances (Å) and angles (°) of **2a** and **2b** **p. 11**
- **Fig. S9** a) Simulated absorption spectra of **2a** and **2b** in water and in acetonitrile; b) Natural Transition Orbitals involved in selected transitions of **2a**; c) Main MOs contribution to each band in acetonitrile and theoretical assignment **p. 12**
- **Fig. S10** Emission spectrum of **2b** in acetonitrile solution at 77K **p. 13**
- **Fig. S11** a) Optimized structures of [(bipy-OH)Cu(Trop)(Sac)] compounds obtained for coordination of saccharinate through carbonyl (named CO), sulfonyl (named SO) and imide (named N) sites; b) Singly Occupied Molecular Orbital (SOMO) and Lowest Unoccupied Molecular Orbitals (LUMO) obtained for the three compounds **p. 13**
- **Fig. S12** Free energy profiles in protein environment (ε = 4) for a) cysteine and b) imidazole substitution reaction of saccharinate on metal centre **p. 14**

Experimental Section

Materials and methods

All commercially available starting materials were used as received without further purification. The 4,4'-bis(hydroxymethyl)-2,2'-bipiridine (bipy-OH) has been synthesized according to a procedure previously described.[1]

Physical techniques

Infrared spectra were recorded with a Perkin-Elmer Spectrum One FT-IR spectrometer (KBr pellets). ^{1}H-NMR spectra were acquired on a Bruker Avance 300 MHz spectrometer in D_2O solution (with TMS as the internal standard). Elemental analyses were performed with a Perkin-Elmer 2400 microanalyzer by the Microanalytical Laboratory at University of Calabria. Conductivity measurements were performed in solutions with an InoLab Cond Level 1-720 conductometer equipped with LR 325-001 immersion cell. Powder X-ray diffraction patterns of the bulk samples were acquired on a Bruker D2-Phaser equipped with Cu K_α radiation (λ = 1.5418 Å) and a Lynxeye detector, at 30 kV and 10 mA, with a step size of 0.01° (2θ), over an angular range of 5–45° 2θ.

Spectrofluorimetric grade acetone (Acros Organics) was used for the photophysical investigations in solution. Steady-state emission spectra were recorded on a Horiba Jobin Yvon Fluorolog 3 spectrofluorimeter, equipped with a Hamamatsu R-928 photomultiplier tube. Emission quantum yields of sample in solution were determined using the optically dilute method on deaerated solutions whose absorbance at excitation wavelengths was <0.1; $Ru(bipy)_3Cl_2$ (bipy = 2,2'-bipyridine) in H_2O was used as standard (Φ = 0.028).[2] The experimental uncertainty on the emission quantum yields is 10%.

The spectrophotometric measurements to determine the solubility of the compounds have been conducted with a Varian Cary 50 Scan UV-Visible Spectrophotometer. The temperature of the cell-holder was kept at 298.15 K by a Grant circulating water bath. Matched quartz cells of thickness 1 cm were employed. The absorbance, A_λ, were recorded to ± 0.0001 units. The formulations of the parameters and the acquisition of the data have been managed with the aid of a computer connected to the tool. The solubility (S, mol/dm^3) of the compounds was evaluated, at 298.15 K, in pure water by spectrophotometric measurements in the UV-Vis region. All solutions were prepared using ultrapure water, with a resistivity of 18.2 MΩ cm, obtained from a Milli-Q plus system (Millipore, Bedford, MA). Saturated compounds solutions were prepared with a leaching apparatus suitable to prevent solid particles from coming into contact with the magnetic stirrer. As a matter of fact, preliminary measurements showed an increase of solubility over periods of weeks when the solid was in mechanical contact with the stirrer, because the solid was transformed into a dispersed phase. To avoid grinding by the stirrer, solid compounds were wrapped up in a highly retentive filter paper (Whatman 42) bag. This in turn was kept in a glass cylinder containing pure water while continuously stirring with a magnetic bar. The experimental apparatus is reported in Fig. S1. Finally, the absorption spectra in the UV-Vis region were recorded on a series of compounds solutions.

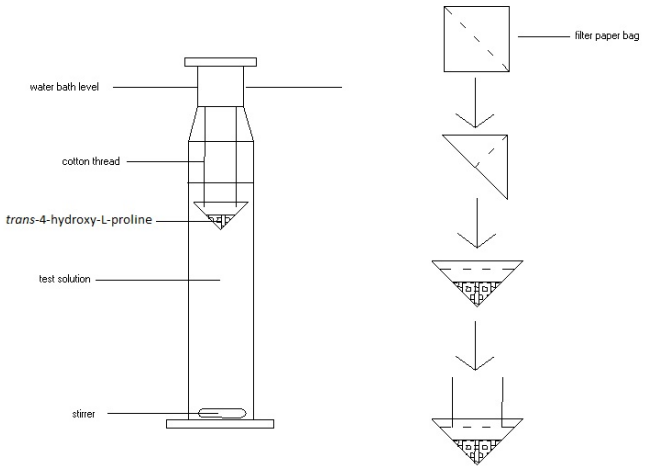

Fig. S1 Apparatus for preparation of saturated compounds solution.

The cylinder was then placed in a thermostatic water bath at 298.15 K and the compounds concentrations were monitored over the time, until it reached a constant value, which usually occurred in about 4 days. Finally, the absorption spectra in the UV-Vis region were recorded on a series of compounds solutions. Taking as a blank the pure water, the absorbance, A_λ, may be expressed as equation 1:

$$A_\lambda = l\,\varepsilon\,[\mathrm{cpx}] \qquad (1)$$

where [cpx] is the equilibrium concentration of the compounds, l is the optical path and ε is the molar absorbivity. A_λ were measured between 190 and 780 nm to find suitable conditions for determining the solubility, S, of the compounds. Three replicates were run for each point. A typical spectrum of the compounds recorded is reported in Fig. S2.

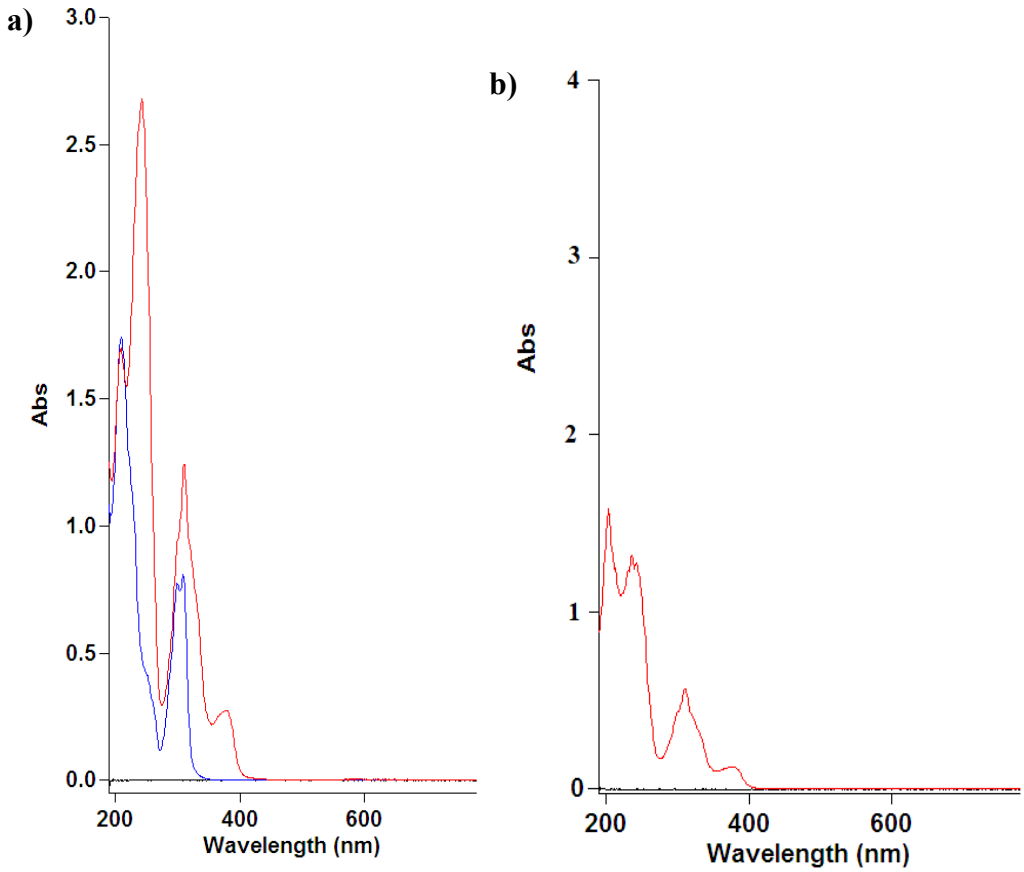

Fig. S2 Absorption spectrum for **1a** (blue line), **1** (red line) (a) and **2** (b).

As it can be seen, the absorption spectra of the compounds show different bands at different intensities. The most intense peak at 200 nm seems the most suitable, its reproducibility is however very poor. On the contrary, the peaks at 309, 378 and 377 nm, for **1a**, **1** and **2** respectively, were considered more adequate for accurate determinations. The solubility, *S*, for each complex was deduced by interpolation on a calibration curve, based on standard solutions. The reproducibility of the solubility data was of 1%.

Preparation of 1a, 1, 2a and 2b

[(bipy-OH)CuCl$_2$]$_\infty$·H$_2$O, 1a. 1.5 equivalents of $CuCl_2 \cdot 2H_2O$ (0.12 g, 0.69 mmol) was added to a solution of [(bipy-OH)] (0.1 g, 0.46 mmol) in hot acetone (50 ml). After stirring for 1 d the solution was filtered and a green-blue solid washed in acetone (89 % yield). Mp 267 °C$_{dec}$. Anal. Calc. for $C_{12}H_{14}O_3N_2CuCl_2$: C, 39.09; H, 3.83; N, 7.60. Found: C, 39.17; H, 3.93; N, 7.72. IR (KBr) ν_{max}/cm^{-1}: 3433 (OH), 3053 (C-H), 1616 (C=C), 1488 (C=N). Λ_{water}= 190.03 $\Omega^{-1}\cdot cm^2\cdot mol^{-1}$. Water solubility, $S\cdot 10^3$ = 2.58 µM (mol/dm^3).

[(bipy-OH)Cu(Trop)(Cl)]·H$_2$O, 1. A solution of Potassium Tropolonate (0.02g, 0.136mmol) in methanol (3mL) was added very slowly and dropwise to a solution of **1a** (0.05g, 0.136 mmol) in an ice bath (5.5mL). The resulting green solution was allowed to stir at room temperature and under nitrogen for 24 h. Subsequently, the solvent was evaporated in *vacuo.* The product was recrystallized by methanol/ether ethylic to give a green solid (97% yield). Mp 234°C$_{dec}$. Anal. Calc. for $C_{19}H_{19}O_5N_2CuCl$: C, 50.22; H, 4.21; N, 6.17. Found: C, 50.45; H, 4.11; N, 6.20. IR (KBr) ν_{max}/cm^{-1}: 3339 (OH), 3022 (C-H), 2901 (C-H), 1620 (C=C), 1592 (C=O), 1515 (C=N). Λ_{warer}= 100.1 $\Omega^{-1}\cdot cm^2\cdot mol^{-1}$. Water solubility, $S\cdot 10^3$ = 5.36 µM (mol/dm^3).

[(bipy-OH)Cu(Trop)Sac], 2a

Solid state reaction. [(bipy-OH)Cu(Trop)Cl], **1** (0.03g, 0.06 mmol), saccharin (0.03g, 0.131mmol) and water (100µL) have been grinded in a ball mill for 4h. The so obtained blue powder has been dissolved in water and, from slow evaporation after few days, dark blue crystals have been obtained in very high yield (96%). Mp 220°C_{dec} Anal. Calc. for $C_{26}H_{21}N_3CuO_7S$: C, 53.56; H, 3.63; N, 7.21. Found: C, 53.24; H, 3.76; N, 7.26. IR (KBr) ν_{max}/cm^{-1}: 3508 (OH), 3182 (C-H), 2912 (C-H), 1630 (C=O, Sac), 1593 (C=O, Trop), 1581 (C=C), 1513 (C=N), 1253 (ν_{as} SO_2), 1136 (ν_s SO_2). Λ_{water}= 41.24 $\Omega^{-1}\cdot cm^2\cdot mol^{-1}$. Water solubility, $S\cdot 10^3$ = 2.15 µM (mol/dm^3).

Solution reaction. **1** (0.05 g, 0.11 mmol) was added to a water solution of saccharin (0.02 g, 0.11 mmol). The resulting mixture was stirred for 24 h; then for slow evaporation, blue crystals have been separated, resulting, through single crystal X ray diffraction analysis, the same product obtained in the solid-state reaction.

[(bipy-OH)Cu(Trop)Sac]·H_2O, 2b

Rotary evaporation reaction. **1** (0.05 g, 0.11 mmol) was added to a water solution of saccharin (0.02 g, 0.11 mmol). The resulting mixture was stirred for 1 h; then the solvent was fast evaporated though a rotary evaporator yielding a green solid. Green crystals were obtained by slow evaporation of a water solution of the isolated crystalline green powder and then analyzed through single crystal X ray diffraction.

X ray crystallographic analysis

Single crystal X ray diffraction data of **1a-1** and **2a-2b** were collected at room temperature with a Bruker-Nonius X8APEXII CCD area detector system equipped with a graphite monochromator with radiation Mo Kα (λ = 0.71073 Å). These data were processed through the SAINT[3] reduction and SADABS[4] absorption software. The structures were solved by direct methods and refined by full-matrix least-squares based on F^2through the *SHELX* and *SHELXTL* structure determination package.[5] Generally, all non-hydrogen atoms were refined anisotropically and hydrogen atoms were included as idealized riding atoms. All graphical representations have been obtained by using Olex2 Software Package (Version 1.3.0)[6] and CCDC Mercury 4.3.0. Details of data and structure refinements are given in Table S1.

Table S1 Details of data collection and structure refinements for **1a-1** and **2a-2b**

	1a	1	2a	2b
formula	$C_{12}H_{16}Cl_2CuN_2O_4$	$C_{19}H_{19}ClCuN_2O_5$	$C_{26}H_{21}CuN_3O_7S$	$C_{26}H_{23}CuN_3O_8S$
Mr	386.71	454.35	583.06	601.07
crystal size [mm]	0.19 x 0.15 x 0.10	0.22 x 0.18 x 0.12	0.23 x 0.17 x 0.12	0.15 x 0.11 x 0.08
crystal system	Monoclinic	Triclinic	Triclinic	Triclinic
space group	*P*2/*n*	*P*-1	*P*-1	*P*-1
a [Å]	6.9309(11)	9.109(2)	10.555(5)	10.4833(7)
b [Å]	9.6019(15)	10.048(3)	10.670(4)	10.9633(9)
c [Å]	11.0089(18)	11.646(3)	11.522(5)	11.1057(9)
α [°]	90	70.788(12)	87.02(3)	86.33(4)
β [°]	93.855(9)	75.475(13)	88.25(3)	87.40(4)
γ [°]	90	75.667(13)	68.34(3)	81.78(4)
V [Å^3]	731.0(2)	958.4(4)	4992.5(16)	1259.8(2)
Z	2	2	2	2
ρ cald [gcm^{-3}]	1.757	1.574	1.608	1.584
μ [mm^{-1}]	1.875	1.313	1.048	1.007
ϑ range [°]	2.121-29.574	1.884-26.369	2.056-25.348	2.521-26.594
data collected	15801	15255	16495	22203
unique data, R_{int}	2066, 0.0309	3860, 0.0379	4353, 0.0486	5216, 0.0315
obs. data [$I > 2\sigma(I)$]	1802	2975	3243	4082
no. parameters	270	270	343	358
R_1 [obs. data]	0.0277	0.0427	0.0364	0.0440
wR_2 [all data]	0.0768	0.0924	0.0917	0.1322
GOF	1.003	1.105	1.049	1.024

Hydrogen bond propensity calculations

Hydrogen Bond Propensity calculation have been performed starting by using the Material Science module available as part of Mercury 2020.1 software from the Cambridge Crystallographic Data Centre (CCDC) with version 4.41 of the Cambridge Structural Database. The target molecule of complex 2a was sketched and auto-edited, functional groups were selected as suggested by Mercury, a training dataset (between 300 and 600 structures per functional group; total hits selected for training dataset 599, good size) was made, and the propensity values were calculated using a logistic regression model with an area under ROC curve of 0.802 ("good discrimination").

The propensity score for all donor/acceptor combinations is calculated from the average of the contributing propensity scores, as well as the coordination score is the average of the coordination scores contributing to the permutation of donors and acceptors. A statistical model based on the likelihood that a functional group participates 0, >1, >2 times. Is used in the calculation of the coordination scores.

Computational details

The optimizations of all Cu-containing complexes have been performed by employing the hybrid B3LYP exchange–correlation functional [7,8]including the dispersion contributions D3 for non-bonding interaction.[9] The standard triple-ζ 6-311+G** basis set has been used for O and N atoms and 6-

311G** for the others, while the SDD pseudo-potential, coupled with its spit valence basis set,[10] has been employed for metal ion. The relative stability of all the investigated copper complexes has been determined as energy difference between the obtained adduct [(bipy-OH)Cu(Trop)(Sac)] and the sum of the energy of $[bipy\text{-}OH)Cu(Trop)]^{+}$ complex and saccharinate ion. As all the copper-containing species are in a doublet state, the unrestricted Kohn–Sham (UKS) formalism has been used for all the calculations. For these optimizations, the aqueous environment has been modeled with the polarized continuum model using the integral equation formalism variant (IEFPCM)[11,12] and the UFF set of radii has been selected to build up the cavity.

The reaction pathways have been obtained by performing the optimization of all the involved minima and transition states at the DFT level described above coupled with the standard double-ζ 6-31+G* basis for the atoms directly coordinated to Cu^{II} metal ion and 6-31G** for the others, whose energies were refined with a single point calculation using 6-311++G** for all the atoms, except metals for which the SDD pseudo-potential was retained. In such cases, the protein environment was simulated by means of the polarizable continuum model, using a dielectric constant value of 4, suggested for taking into account the coupled effect of the protein itself and the water medium surrounding the protein.[13]

Vibrational analysis was used to obtain the zero point corrections and to check the nature of all the stationary points along the described pathway: transition states, only one imaginary frequency, and intermediates, no imaginary frequency. All the computations were carried out using Gaussian 09 code.[14]

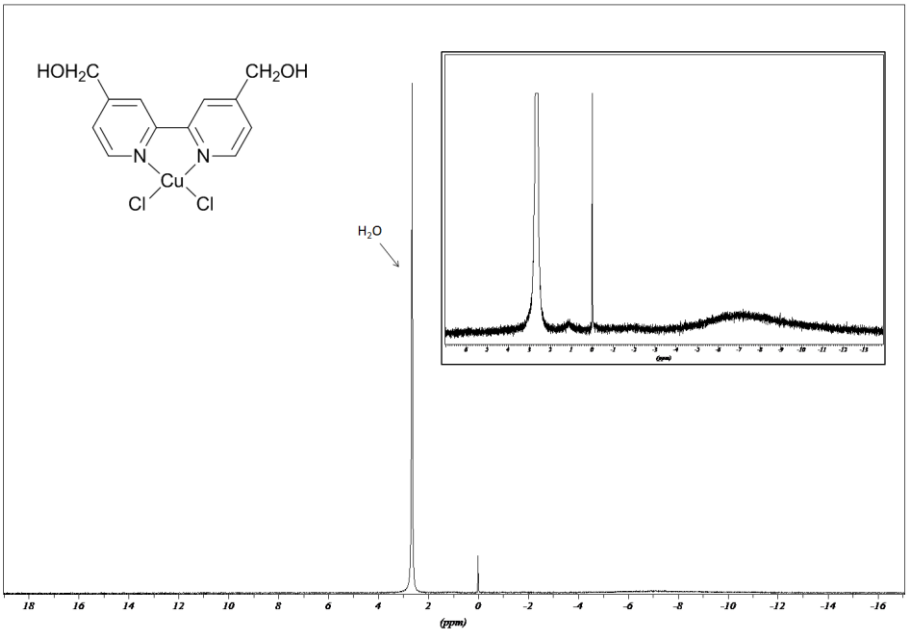

Fig. S3 ^{1}H-NMR spectrum of **1a.**

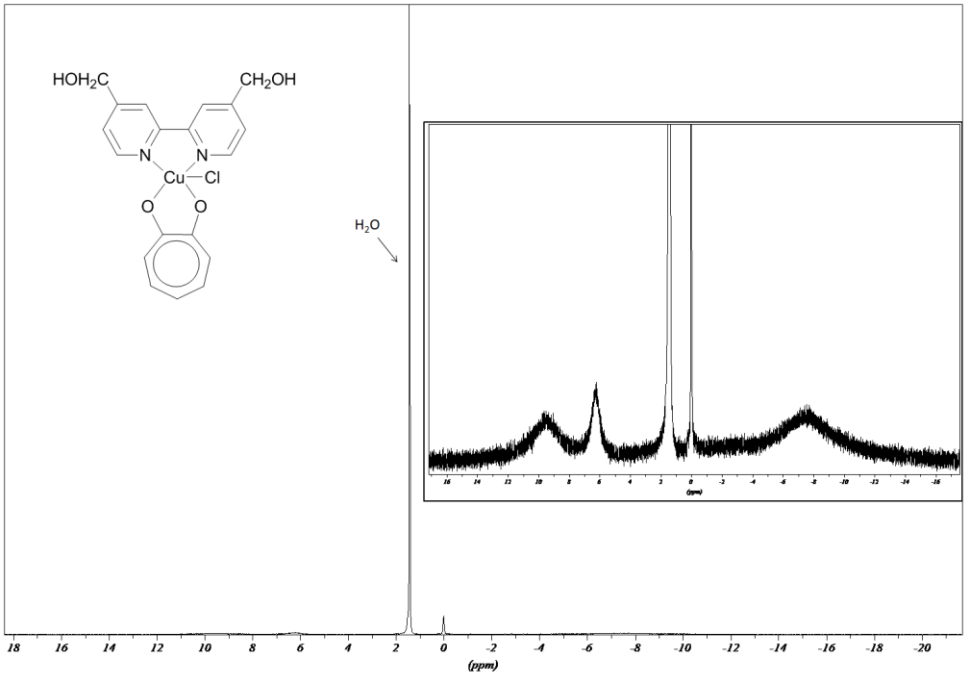

Fig. S4 ^{1}H-NMR spectrum of **1.**

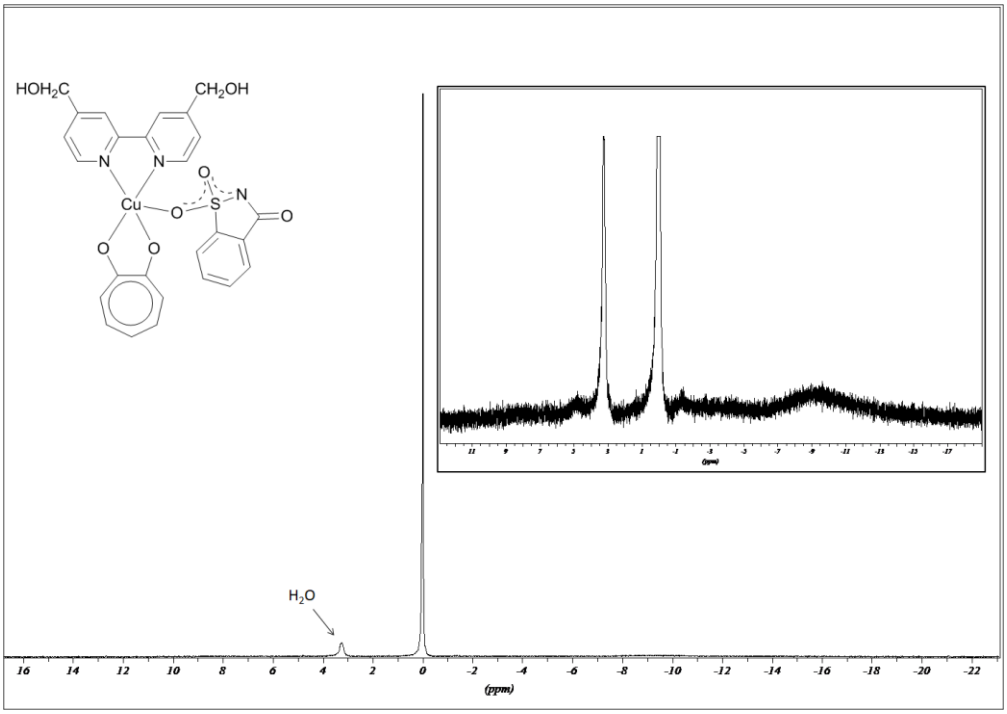

Fig. S5 ^{1}H-NMR of **2**.

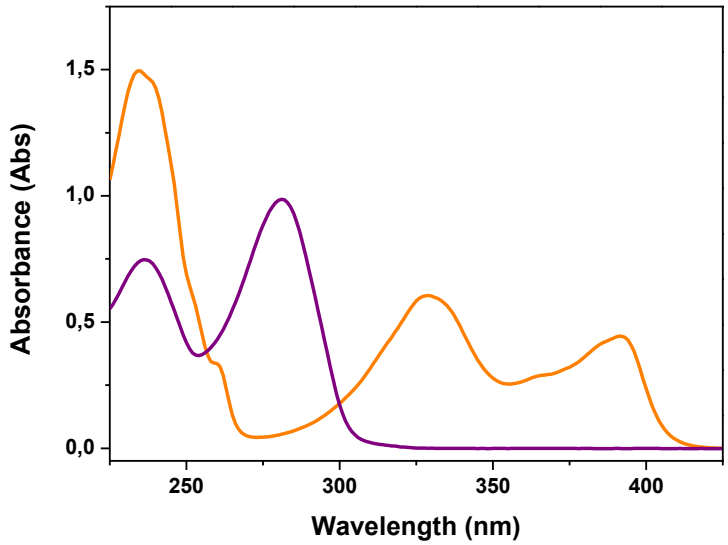

Fig. S6 Absorption spectra of tropolone (orange trace) and 2,2'-bipyridine (purple trace) in water solution at room temperature.

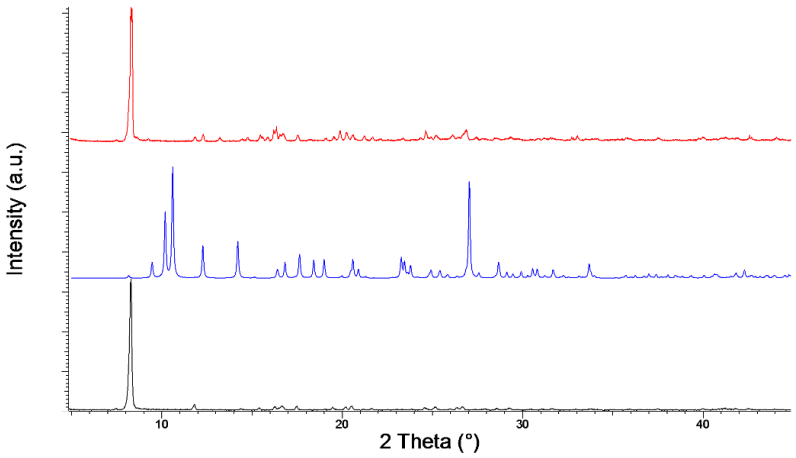

Fig. S7 Comparison between the X-ray powder pattern (black) measured on the pale-blue powder of **1a**, (blue) calculated from the single crystal data and (red) measured on the needle-shaped microcrystals.

Table S2 Selected bond distances (Å) and angles (°) of **1** and [(bipy-OH)Zn(Trop)(Cl)][15]

	1	**[(bipy-OH)Zn(Trop)(Cl)]**
M-O(1)	1.933(3)	2.026(1)
M-O(2)	1.922(3)	2.049(1)
M-N(1)	1.980(3)	2.096(1)
M-N(2)	1.974(3)	2.103(1)
M-Cl	2.7375(12)	2.2717(6)
Cl-M-O(1)	98.76(9)	105.87(4)
Cl-M-O(2)	99.92(8)	107.49(4)
Cl-M-N(1)	87.82(9)	105.53(4)
Cl-M-N(2)	91.86(9)	105.73(4)
O(1)-M-O(2)	83.35(10)	78.61(5)
N(1)-M-N(2)	82.12(12)	77.44(5)
O(1)-M-N(1)	98.34(11)	93.97(5)
O(1)-M-N(2)	169.38(12)	148.40(5)
O(2)-M-N(1)	171.76(12)	146.93(6)
O(2)-M-N(2)	94.73(11)	92.07(5)

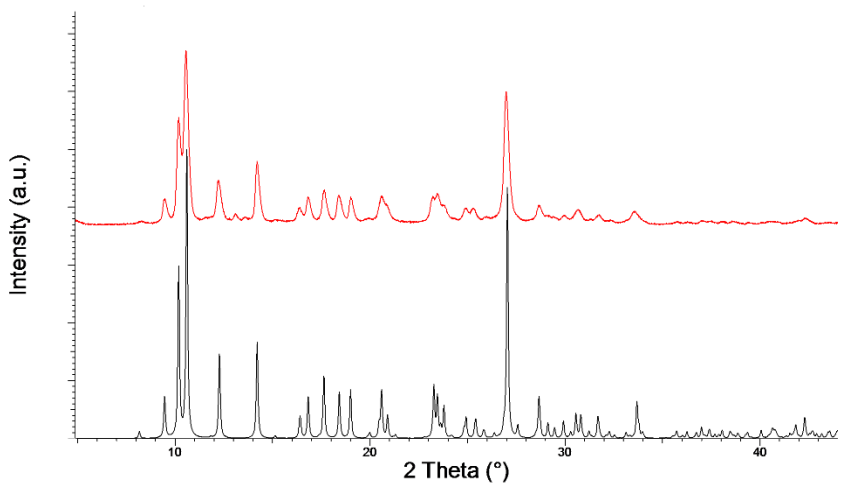

Fig. S8 Comparison between the X-ray powder pattern (black) calculated from the single crystal data of **1** and (red) measured on blue powder.

Table S3	**Selected bond distances (Å) and angles (°) of, 2a and 2b**	
	2a	**2b**
Cu-O(1)	1.941(2)	1.931(2)
Cu-O(2)	1.935(2)	1.919(2)
Cu-N(1)	1.977(2)	1.961(2)
Cu-N(2)	1.989(2)	1.983(3)
Cu-O(4)	2.529(2)	2.534(3)
O(1)-Cu-O(2)	84.06(8)	83.74(9)
N(1)-Cu-N(2)	82.14(9)	81.77(10)
O(1)-Cu-N(1)	96.52(9)	97.22(10)
O(1)-Cu-N(2)	171.94(9)	174.2910)
O(2)-Cu-N(1)	178.94(8)	178.4910)
O(2)-Cu-N(2)	97.41(9)	97.38(10
O(1)-Cu-O(4)	93.17(8)	95.47(8)
O(2)-Cu-O(4)	83.38(8)	87.25(9)
N(1)-Cu-O(4)	95.70(9)	91.48(9)
N(2)-Cu-O(4)	94.87(8)	90.188)

a)

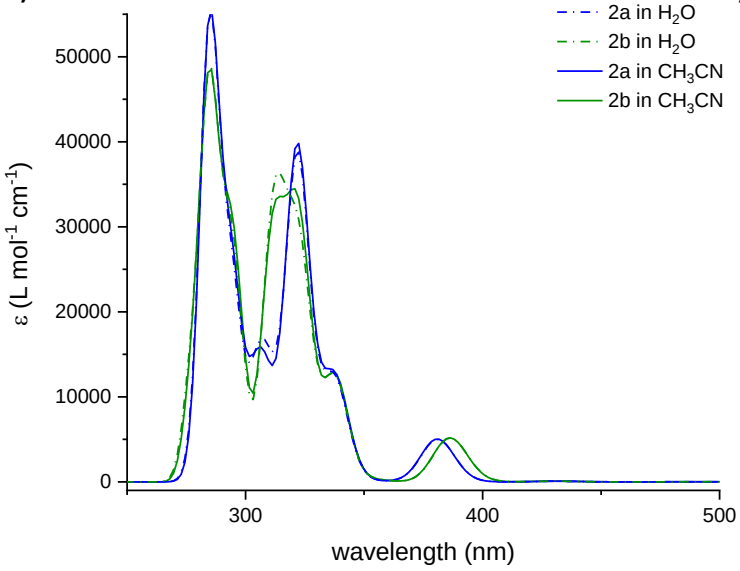

b)

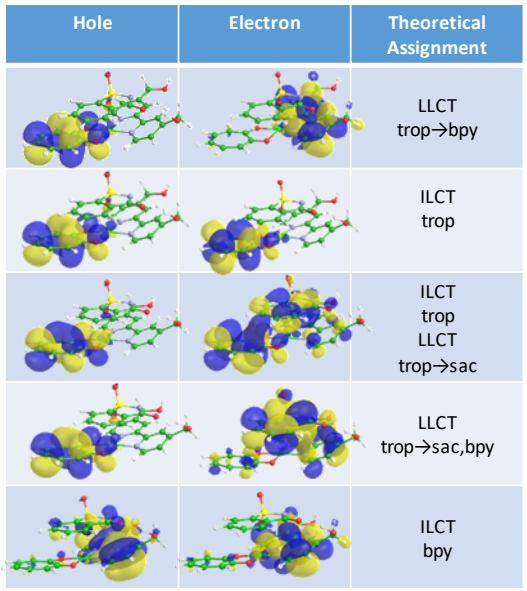

c) **Band** (in CH_3CN)	**λ (nm)**	**MOs contribution, %**	***f***
		2a (**2b**)	
LLCT *trop→bipy*	380 (385)	Hα → Lα, 94% (Hα → Lα, 94%)	0.018 (0.018)
ILCT *trop*	337 (338)	Hα → L+2α, 42%; H-1β → L+2β, 41% (Hα → L+1α, 41%; H-1β → L+1β, 41%)	0.061 (0.057)
ILCT *trop* – **LLCT** *trop→sac*	322 (323)	Hα → L+2α, 38%; H-1β → L+2β, 40% (Hα → L+α, 29%; Hβ → L+2β, 35%)	0.188 (0.120)
LLCT *trop→sac,bipy*	306 (311)	Hα → L+3α, 67% (Hα → L+3α, 58%)	0.044 (0.119)
ILCT *bipy*	294 (296)	H-2β → L+1β, 29%; H-2α → Lα, 20% (H-2β → L+1β, 26%; H-2α → Lα, 19%)	0.102 (0.071)

Fig. S9 a) Simulated absorption spectra of **2a** and **2b** in water and in acetonitrile; b) Natural Transition Orbitals involved in selected transitions of **2a**; c) Main MOs contribution to each band in acetonitrile and theoretical assignment.

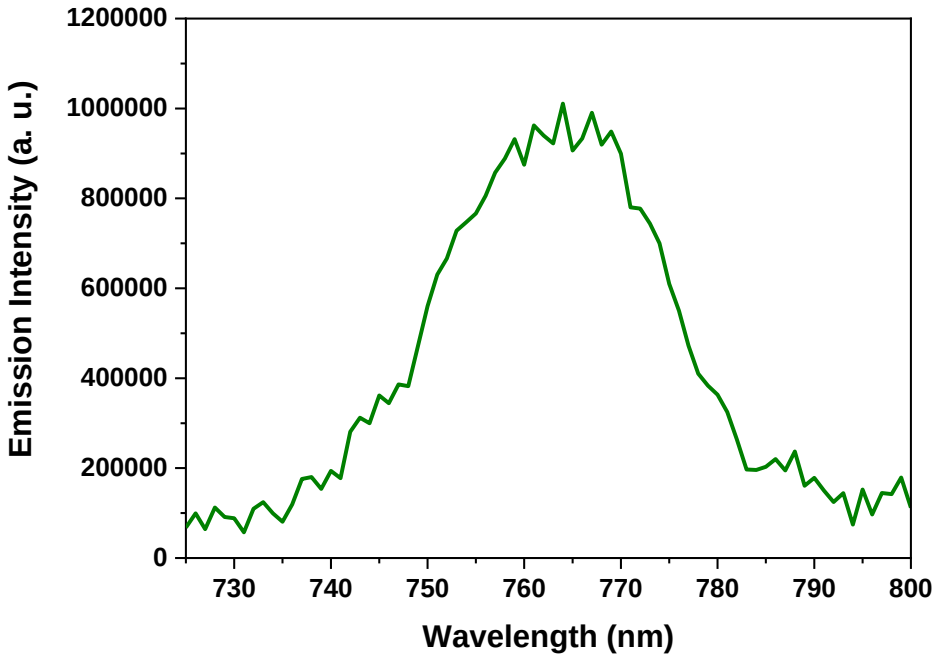

Fig. S10 Emission spectrum of **2b** in acetonitrile solution at 77K. Spectrum recorded from **2a** is superimposable.

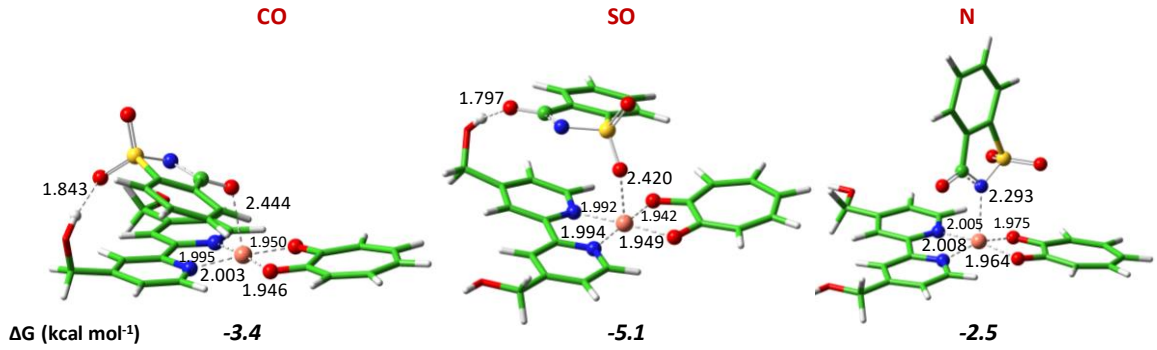

Fig. S11 Optimized structures of [(bipy-OH)Cu(Trop)(Sac)] compounds obtained for coordination of saccharinate through carbonyl (named CO), sulfonyl (named SO) and imide (named N) sites.

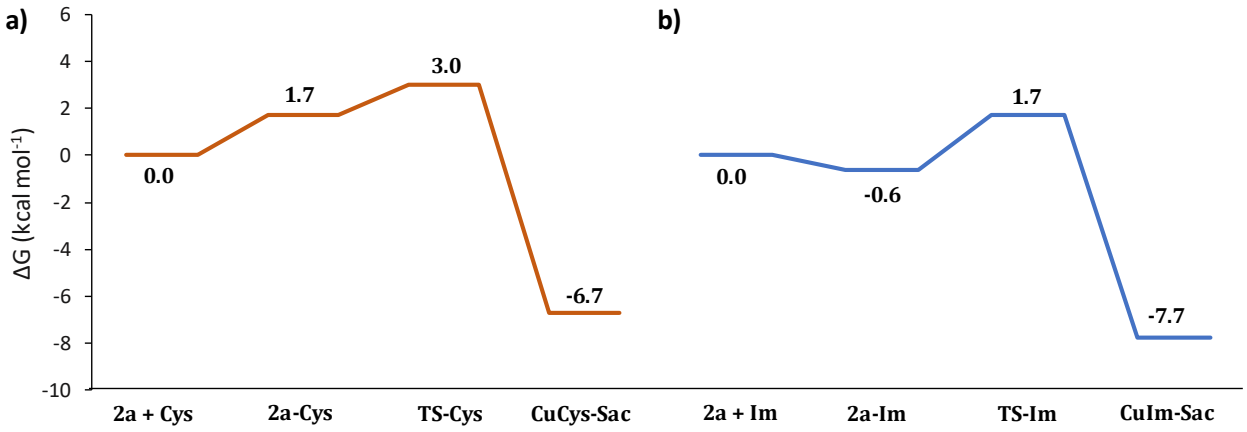

Fig. S12 Free energy profiles in protein environment (ε = 4) for a) cysteine and b) imidazole substitution reaction of saccharinate on metal centre.

References

1 G. Will, G. Boschloo, S. Nagara Rao and D. Fitzmaurice, Potentiostatic modulation of the lifetime of light-induced charge separation in a heterosupermolecule, *J. Phys. Chem. B*, 1999, **103**, 8069-8079.

2 K. Nakamaru, Synthesis, luminescence quantum yields, and lifetimes of trischelated ruthenium (II) mixed-ligand complexes including 3, 3′-dimethyl-2, 2′-bipyridyl, *Bull. Soc. Chem. Jpn.*, 1982, **5**, 2697-2705.

3 SAINT, Version 6.45 Copyright 2003, Bruker Analytical -ray Systems Inc.

4 G.M Sheldrick, SADABS. Version 2.10, Bruker AXS Inc., Madison, USA, 2003

5 G. M. Sheldrick, A short history of SHELX, *Acta Cryst.,* 2008, A**64**, 112-122.

6 O. V. Dolomanov, L. J. Bourhis, R.J. Gildea, J. A. K. Howard and H. Puschmann, OLEX2: a complete structure solution, refinement and analysis program, *J. Appl. Cryst.*, 2009, **42**, 339-341.

7 C. Lee, W. Yang and R. G. Parr, Development of the Colle-Salvetti correlation-energy formula into a functional of the electron density, *Phys. Rev. B*, 1988, **37**, 785-789.

8 S. Grimme, J. Antony, S. Ehrlich and H. Krieg, A consistent and accurate ab initio parametrization of density functional dispersion correction (DFT-D) for the 94 elements H-Pu, *J. Chem. Phys.*, 2010, **132**, 154104.

9 D. Andrae, U. Häußermann, M. Dolg, H. Stoll and H. Preuß, A consistent and accurate ab initio parametrization of density functional dispersion correction (DFT-D) for the 94 elements H-Pu, *Theoret. Chim. Acta*, 1990, **77**, 123-141.

10 S. Miertuš and J. Tomasi, Approximate evaluations of the electrostatic free energy and internal energy changes in solution processes, *Chem. Phys.*, 1982, **65**, 239-245.

11 S. Miertuš, E. Scrocco and J. Tomasi, Electrostatic interaction of a solute with a continuum. A direct utilization of AB initio molecular potentials for the prevision of solvent effects, *Chem. Phys.*, 1981, **55**, 117-129.

12 M. Frisch, G. Trucks, H. Schlegel, G. Scuseria, M. Robb, J. Cheeseman, G. Scalmani, V. Barone, B. Mennucci, G. Petersson, H. Nakatsuji, M. Caricato, X. Li, H. Hratchian, A. Izmaylov, J. Bloino, G. Zheng, J. Sonnenberg, M. Hada, M. Ehara, K. Toyota, R. Fukuda, J. Hasegawa, M. Ishida, T. Nakajima, Y. Honda, O. Kitao, H. Nakai, T. Vreven, J. Montgomery, J. Peralta, F. Ogliaro, M. Bearpark, J. Heyd, E. Bothers, K. Kudin, V. Staroverov, R. Kobayashi, J. Normand, K. Raghavachari, A. Rendell, J. Burant, S. Iyengar, J. Tomasi, M. Cossi, N. Rega, J. Millam, M. Klene, J. Knox, J. Cross, V. Bakken, C. Adamo, J. Jaramillo, R. Gomperts, R. Stratmann, O. Yazyev, A. Austin, R. Cammi, C. Pomelli, J. Ochterski, R. Martin, K. Morokuma, V. Zakrzewski, G. Voth, P.

Salvador, J. Dannenberg, S. Dapprich, A. D. Farkas, J. Foresman, J. Ortiz, J. Cioslowski and D. Fox, *Gaussian 09, Revision B.01, Gaussian, Inc., Wallingford CT.*

13 M. R. A. Blomberg, T. Borowski, F. Himo, R.-Z. Liao and P. E. M. Siegbahn, Quantum Chemical Studies of Mechanisms for Metalloenzymes, *Chem. Rev.*, 2014, **114**, 3601-3658.

14 B. P. Mahon, A. M. Hendon, J. M. Driscoll, G. M. Rankin, S.-A. Poulsen, C. T. Supuran and R. McKenna, Saccharin: A lead compound for structure-based drug design of carbonic anhydrase IX inhibitors, *Bioorg. Med. Chem*., 2015, **23**, 849-854.

15 B. Sanz Mendiguchia, D. Pucci, T. F. Mastropietro, M. Ghedini and A. Crispini, Non-classical anticancer agents: on the way to water soluble zinc (II) heteroleptic complexes, *Dalton Trans.*, 2013, **42**, 6768-6774.